J|A|C|S ARTICLES

Published on Web 07/16/2010

Synthesis, Morphological Control, and Antibacterial Properties of Hollow/Solid Ag_2S/Ag Heterodimers

Maolin Pang,[†] Jiangyong Hu,[‡] and Hua Chun Zeng*,[†]

Department of Chemical and Biomolecular Engineering, KAUST-NUS GCR Program, and Division of Environmental Science and Engineering, Faculty of Engineering, National University of Singapore, 10 Kent Ridge Crescent, Singapore 119260

Received March 11, 2010; E-mail: chezhc@nus.edu.sg

Abstract: Ag_2S and Ag are important functional materials that have received considerable research interest in recent years. In this work, we develop a solution-based synthetic method to combine these two materials into hollow/solid Ag_2S/Ag heterodimers at room temperature. Starting from monodisperse Cu_2O solid spheres, CuS hollow spheres can be converted from Cu_2O through a modified Kirkendall process, and the obtained CuS can then be used as a solid precursor for preparation of the Ag_2S/Ag heterodimers through ion exchange and photo-assisted reduction. We have found that formation of the Ag_2S/Ag heterodimers is instantaneous, and the size of Ag nanocrystals on the hollow spheres of Ag_2S can be controlled by changing the concentration and power of reducing agents in the synthesis. The growth of Ag nanoparticles on hollow spheres of Ag_2S in the dimers is along the [111] direction of the silver crystal; the light absorption properties have also been investigated. Furthermore, coupling or tripling of Ag_2S/Ag heterodimers into dumbbell-like trimers (($Ag_2S)_2$/Ag, linear) and triangular tetramers (($Ag_2S)_3$/Ag, coplanar) can also be attained at 60 °C by adding the bidentate ligand ethylenediamine as a cross-linking agent. To test the applicability of this highly asymmetric dipolar composite, photocatalytic inactivation of *Escherichia coli* K-12 in the presence of the as-prepared Ag_2S/Ag heterodimers has been carried out under UV irradiation. The added Ag_2S/Ag heterodimers show good chemical stability under prolonged UV irradiation, and no appreciable solid dissolution is found. Possible mechanisms regarding the enhanced antibacterial activity have also been addressed.

1. Introduction

In recent years, synthetic approaches to the preparation of nanocomposite materials have attracted significant research interest in the nanochemistry community. The investigated nanocomposites consist of two or more material phases, and therefore their different physicochemical functionalities promise potential applications across vast fields of medicine, catalysis, optoelectronic devices, etc.[1−23] A great number of binary and/or ternary composites with tunable particle size in the nanoscale regime and controllable morphology have already been synthesized by spontaneous nucleation and growth or direct

[†] Department of Chemical and Biomolecular Engineering.
[‡] Division of Environmental Science and Engineering.

(1) (a) Mokari, T.; Rothenberg, E.; Popov, I.; Costi, R.; Banin, U. *Science* **2004**, *304*, 1787. (b) Mokari, T.; Sztrum, C. G.; Salant, A.; Rabani, E.; Banin, U. *Nat. Mater.* **2005**, *4*, 855.
(2) (a) Cozzoli, P. D.; Pellegrino, T.; Manna, L. *Chem. Soc. Rev.* **2006**, *35*, 1195. (b) Casavola, M.; Buonsanti, R.; Caputo, G.; Cozzoli, P. D. *Eur. J. Inorg. Chem.* **2008**, *6*, 837.
(3) Pellegrino, T.; Fiore, A.; Carlino, E.; Giannini, C.; Cozzoli, P. D.; Ciccarella, G.; Respaud, M.; Palmirotta, L.; Cingolani, R.; Manna, L. *J. Am. Chem. Soc.* **2006**, *128*, 6690.
(4) Shi, W. L.; Zeng, H.; Sahoo, Y.; Ohulchanskyy, T. Y.; Ding, Y.; Wang, Z. L.; Swihart, M.; Prasad, P. N. *Nano Lett.* **2006**, *6*, 875.
(5) Yu, H.; Chen, M.; Rice, P. M.; Wang, S. X.; White, R. L.; Sun, S. H. *Nano Lett.* **2005**, *5*, 379.
(6) Yang, J.; Elim, H. I.; Zhang, Q.; Lee, J. Y.; Ji, W. *J. Am. Chem. Soc.* **2006**, *128*, 11921.
(7) Gu, H.; Yang, Z.; Gao, J.; Chang, C. K.; Xu, B. *J. Am. Chem. Soc.* **2005**, *127*, 34.
(8) Jiang, J.; Gu, H. W.; Shao, H. L.; Devlin, E.; Papaefthymiou, G. C.; Ying, J. Y. *Adv. Mater.* **2008**, *20*, 4403.
(9) Yang, J.; Ying, J. Y. *Chem. Commun.* **2009**, 3187.
(10) Lu, Y.; Xiong, H.; Jiang, X. C.; Xia, Y. N.; Prentiss, M.; Whitesides, G. M. *J. Am. Chem. Soc.* **2003**, *125*, 12724.
(11) Habas, S. E.; Lee, H.; Radmilovic, V.; Somorjai, G. A.; Yang, P. *Nat. Mater.* **2007**, *6*, 692.
(12) Buonsanti, R.; Grillo, V.; Carlino, E.; Giannini, C.; Curri, M. L.; Innocenti, C.; Sangregorio, C.; Achterhold, K.; Parak, F. G.; Agostiano, A.; Cozzoli, P. D. *J. Am. Chem. Soc.* **2006**, *128*, 16953.
(13) Kudera, S.; Carbone, L.; Casula, M. F.; Cingolani, R.; Falqui, A.; Snoeck, E.; Parak, W. J.; Manna, L. *Nano Lett.* **2005**, *5*, 445.
(14) Figuerola, A.; Fiore, A.; Di Corato, R.; Falqui, A.; Giannini, C.; Micotti, E.; Lascialfari, A.; Corti, M.; Cingolani, R.; Pellegrino, T.; Cozzoli, P. D.; Manna, L. *J. Am. Chem. Soc.* **2008**, *130*, 1477.
(15) Carbone, L.; et al. *Nano Lett.* **2007**, *7*, 2942.
(16) Casavola, M.; Falqui, A.; Garcia, M. A.; Garcia-Hernandez, M.; Giannini, C.; Cingolani, R.; Cozzoli, P. D. *Nano Lett.* **2009**, *9*, 366.
(17) Casavola, M.; Grillo, V.; Carlino, E.; Giannini, C.; Gozzo, F.; Pinel, E. F.; Garcia, M. A.; Manna, L.; Cingolani, R.; Cozzoli, P. D. *Nano Lett.* **2007**, *7*, 1386.
(18) Gu, H.; Zheng, R.; Zhang, X.; Xu, B. *J. Am. Chem. Soc.* **2004**, *126*, 5664.
(19) (a) Kwon, K. W.; Shim, M. *J. Am. Chem. Soc.* **2005**, *127*, 10269. (b) Kwon, K. W.; Lee, B. H.; Shim, M. *Chem. Mater.* **2006**, *18*, 6357. (c) McDaniel, H.; Shim, M. *ACS Nano* **2009**, *3*, 434.
(20) Buonsanti, R.; Grillo, V.; Carlino, E.; Giannini, C.; Gozzo, F.; Garcia-Hernandez, M.; Garcia, M. A.; Cingolani, R.; Cozzoli, P. D. *J. Am. Chem. Soc.* **2010**, *132*, 2437.
(21) Pacholski, C.; Kornowski, A.; Weller, H. *Angew. Chem., Int. Ed.* **2004**, *43*, 4774.
(22) Gao, X. Y.; Yu, L. T.; MacCuspie, R. I.; Matsui, H. *Adv. Mater.* **2005**, *17*, 426.
(23) Wang, C.; Xu, C.; Zeng, H.; Sun, S. *Adv. Mater.* **2009**, *21*, 3045.

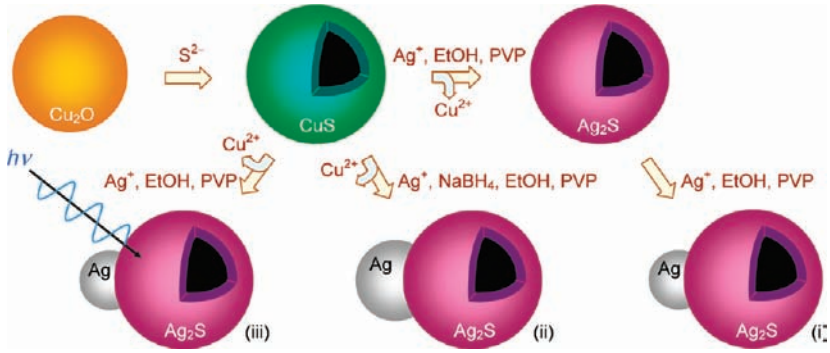

Figure 1. Schematic illustration of the formation of Ag_2S/Ag heterodimers synthesized in the present work: (i) with standard reaction conditions (Experimental Section), (ii) with addition of a strong reducing agent $NaBH_4$, and (iii) with assistance of UV irradiation.

deposition of a second and/or third component onto primary (parent) nanomaterials. In association with these synthetic endeavors, multifunctional nanostructures that combine magnetic, electrical, semiconducting, optical, optoelectronic, and catalytic properties have been realized.[1−23] Among the investigated nanocomposites, bifunctional heterodimers that are composed of a semiconducting or magnetic phase and a noble metal counterpart have received special attention due to the well-known properties and applications of their individual components. Investigations on this type of heterodimers have been widely reported in the literature over the past few years.[1−10] Excellent examples of these novel functional materials include CdSe/Au,[1,2] $CoPt_3$/Au,[3] PbSe/Au,[4] Fe_3O_4/Au,[4,5] PbS/Au,[4,6] Fe_3O_4/Ag,[7,8] and Ag_2S/Au.[9] It is interesting to note that all these heterodimers contain *three* different elemental species. In this regard, it is also quite surprising to note that fabrication of heterodimers of silver sulfide and silver (Ag_2S/Ag) has not been realized yet, although this simpler material combination involves only *two* heteroatomic species (Ag and S) and their structural analogy of Ag_2S/Au has been reported very recently.[9]

Preparation of Ag_2S/Ag heterodimers could be viewed as an important development for future utilization of this pair of functional materials in many applications, including nanoscale optoelectronic and medical devices. For instance, silver sulfide is a direct narrow-band-gap semiconducting material. Owing to its excellent photoelectric and thermoelectric properties and good chemical stability, Ag_2S has been used in a number of commercially available optical and electronic devices.[24,25] In this connection, synthesis of uniform size and shape-controlled Ag_2S nanomaterials with predictable size and morphology becomes an important subject of research, and several methods have been devised to prepare uniform Ag_2S nanocrystals as well as their superlattices.[24−31] More extensively, size- and shape-controlled synthesis of nanostructured Ag has also been investigated because of its significant roles in nanotechnologies such as optics, catalysis, surface-enhanced Raman spectroscopy, biological labeling, and imaging over the past two decades.[32−34] Furthermore, Ag and Ag-based compounds/solids are well-known antibacterial materials due to their high cytotoxicity to microorganisms and outstanding broad-spectrum antimicrobial activity against as many as 12 kinds of bacteria, including *Escherichia coli*.[35,36]

However, as to the simultaneous generation of Ag and Ag_2S nanoparticles, only a few reports could be found in the literature.[37−40] For example, Ag_2S nanocrystals catalyze the reduction of Ag^+ cations by various reductants, such as hydroquinone ($C_6H_4(OH)_2$) or sodium sulfite (Na_2SO_3).[37] This catalytic reduction is further accelerated by light irradiation,[37] and thus the process can also be classified as the photo-assisted reduction of silver ions. The generation of metallic Ag clusters on Ag_2S nanocrystals by the reduction of mobile Ag^+ ions in the Ag_2S nanocrystals with sulfur derivatives has also been reported, in which the proportions in the composite material can be modulated by electron beam irradiation.[38] The formation and disappearance of a nanoscale silver cluster at the apex of the Ag_2S tip via the solid electrochemical reaction have been demonstrated by scanning tunneling microscopy (STM).[39] Moreover, selective formations of Ag and Ag_2S nanocrystals as well as their binary mixtures have been investigated by a modified hot-injection process in which a single-source precursor molecule, Ag(I) monothiobenzoate (Ag(SCOPh)), was used.[40]

To the best of our knowledge, synthesis of Ag_2S/Ag heterodimers or their derivatives has not been explored so far. In this contribution, therefore, we have developed a facile solution-based method for the preparation of Ag_2S/Ag heterodimers at room temperature. The experimental procedures involved in the synthesis are summarized in Figure 1, with special emphasis on the CuS-to-Ag_2S/Ag conversion. Coupling or even tripling

(24) Lim, W. P.; Zhang, Z.; Low, H. Y.; Chin, W. S. *Angew. Chem., Int. Ed.* **2004**, *43*, 5685.
(25) Lou, W. J.; Wang, X. B.; Chen, M.; Liu, W. M.; Hao, J. C. *Nanotechnology* **2008**, *19*, 225607.
(26) Wang, D.; Xie, T.; Peng, Q.; Li, Y. *J. Am. Chem. Soc.* **2008**, *130*, 4016.
(27) Wang, D. S.; Zheng, W.; Hao, C. H.; Peng, Q.; Li, Y. D. *Chem.—Eur. J.* **2009**, *15*, 1870.
(28) Zhuang, Z.; Peng, Q.; Wang, X.; Li, Y. *Angew. Chem., Int. Ed.* **2007**, *46*, 8174.
(29) Gao, F.; Lu, Q. Y.; Zhao, D. Y. *Nano Lett.* **2003**, *3*, 85.
(30) (a) Motte, L.; Billoudet, F.; Lacaze, E.; Pileni, M. P. *Adv. Mater.* **1996**, *8*, 1018. (b) Motte, L.; Billoudet, F.; Lacaze, E.; Douin, J.; Pileni, M. P. *J. Phys. Chem. B* **1997**, *101*, 138.
(31) Du, Y. P.; Xu, B.; Fu, T.; Cai, M.; Li, F.; Zhang, Y.; Wang, Q. B. *J. Am. Chem. Soc.* **2010**, *132*, 1470.
(32) Sun, Y. G.; Xia, Y. N. *Science* **2002**, *298*, 2176.
(33) Xia, Y.; Xiong, Y.; Lim, B.; Skrabalak, S. *Angew. Chem., Int. Ed.* **2009**, *48*, 60.
(34) Xia, Y. N.; Yang, P. D.; Sun, Y. G.; Wu, Y. Y.; Mayers, B.; Gates, B.; Yin, Y. D.; Kim, F.; Yan, Y. Q. *Adv. Mater.* **2003**, *15*, 353.
(35) Kim, J. S.; Kuk, E.; Yu, K. N.; Kim, J.-H.; Park, S. J.; Lee, H. J.; Kim, S. H.; Park, Y. K.; Park, Y. H.; Hwang, C.-Y.; Kim, Y.-K.; Lee, Y.-S.; Jeong, D. H.; Cho, M.-H. *Nanomedicine* **2007**, *3*, 95.
(36) Zhao, G. J.; Stevens, S. E. *Biometals* **1998**, *11*, 27.
(37) Kryukov, A. I.; Stroyuk, A. L.; Zin'chuk, N. N.; Korzhak, A. V.; Kuchmii, S. Y. *J. Mol. Catal. A—Chem.* **2004**, *221*, 209.
(38) Motte, L.; Urban, J. *J. Phys. Chem. B* **2005**, *109*, 21499.
(39) Terabe, K.; Nakayama, T.; Hasegawa, T.; Aono, M. *J. Appl. Phys.* **2002**, *91*, 10110.
(40) Tang, Q.; Yoon, S. M.; Yang, H. J.; Lee, Y.; Song, H. J.; Byon, H. R.; Choi, H. C. *Langmuir* **2006**, *22*, 2802.

of the as-prepared Ag_2S/Ag heterodimers into $(Ag_2S)_2$/Ag or $(Ag_2S)_3$/Ag structures can also be achieved when the organic ligand ethylenediamine (EDA) is introduced. To exploit possible applications for this metal−semiconductor nanocomposite, we have further carried out investigations on its optical properties, formation mechanism, and the photocatalytic inactivation of *E. coli* K-12 under UV-A light irradiation using the as-prepared Ag_2S/Ag as catalyst. It is important to point out that this type of "hollow (Ag_2S part)/solid (Ag part)" heterodimer structure has not been reported yet in the literature. With this additional interior hollowness in one side of the dimers, the prepared Ag_2S/Ag "hollow/solid" pair is believed to be even more asymmetric, compared with its known "solid/solid" counterparts.[2]

2. Experimental Section

2.1. Materials. Following is the information on all chemicals and solvents used in this work: copper(II) nitrate trihydrate ($Cu(NO_3)_2 \cdot 3H_2O$, 99.5%, Merck), sodium hydroxide (NaOH, 99%, Merck), methanol (CH_3OH, AR for analysis, 99.8%, Merck), ethanol (C_2H_5OH, absolute for analysis, ACS, Merck), 2-propanol (C_3H_7OH, 99.99%, Fisher), ethylenediamine (EDA, $C_2H_4(NH_2)_2$, 99 wt %, Merck), hydrazine (N_2H_4, 35 wt % solution in water, Sigma-Aldrich; used for synthesis of Cu_2O solid spheres),[41] sodium borohydride ($NaBH_4$, 99.99%, Sigma-Aldrich), polyvinylpyrrolidone (PVP K30, MW = 40 000, Fluka), ammonium sulfide ($(NH_4)_2S$, 20% aqueous solution, Strem Chemicals), and silver nitrate ($AgNO_3$, AR@(ACS), Mallinckrodt Chemical). All the chemicals and solvents were used as received without further purification.

2.2. Preparation of Ag_2S/Ag Heterodimers. In our synthetic schemes illustrated in Figure 1, Cu_2O solid spheres and CuS hollow spheres were first prepared at room temperature according to wet chemical methods we developed recently.[41] In order to obtain Ag_2S/Ag heterodimers, $AgNO_3$ was selected as a silver source owing to its high solubility. Unless otherwise specified, the molar ratio between $AgNO_3$ and CuS was set at the stoichiometry of formation of Ag_2S, i.e., $AgNO_3$:CuS = 2:1 (i.e., ionic ratio $Ag^+:S^{2-}$ = 2:1) for the charge balance, assuming that there was no loss or conversion of sulfur anions. In a typical synthesis, briefly, 0.10 mL of the CuS hollow spheres (0.10 M in ethanol) was dispersed in 2.0 mL of ethanol, followed by addition of 0.02 g PVP. After the CuS/PVP mixture was stirred for 30 min, 0.20 mL of $AgNO_3$ aqueous solution (0.10 M) was added dropwise, and the mixture was stirred for another 30 min. Upon the addition of $AgNO_3$, black product precipitates (i.e., Ag_2S/Ag heterodimers) were formed instantaneously. The Ag_2S/Ag products were harvested by centrifugation and washed with anhydrous ethanol twice. All the experimental steps were carried out at room temperature. In order to tune the size of the Ag nanoparticles, other chemical reagents, such as reducing agent sodium borohydrate ($NaBH_4$), were also introduced. In particular, after addition of $AgNO_3$ aqueous solution into the above CuS/PVP ethanol mixture, 0.01−1.0 mL of $NaBH_4$ aqueous solution (0.10 M) was further added, and the molar ratio of $NaBH_4:Ag^+$ in these tests was varied from 5:100 to 5:1. In order to accelerate the reaction, a water bath at 60 °C could be used to heat the system. Since irregular Ag nanoparticles were produced when the molar ratio of $NaBH_4:Ag^+$ was equal to or greater than 1:1, an optimal amount of $NaBH_4$ (0.1 mL, molar ratio of $NaBH_4$: Ag^+ = 1:2) was used to ensure the formation of Ag_2S/Ag heterodimers with larger Ag ends but without producing unattached (freestanding) Ag nanoparticles.

2.3. Preparation of $(Ag_2S)_2$/Ag Heterotrimers and $(Ag_2S)_3$/Ag Heterotetramers. In our preparation of $Ag_2S/Ag/Ag_2S$ dumbbell structure (i.e., $(Ag_2S)_2$/Ag heterotrimers) and $(Ag_2S)_3$/Ag heterotetramers, a certain amount of EDA, ranging from 0.01 to 0.10 mL, was added into the above resultant ethanolic suspension of Ag_2S/Ag heterodimers, and the reaction was conducted at 60 °C in a water bath for 2 h. The products were also collected via centrifation and rinsed with anhydrous ethanol solvent two times.

2.4. Instrumentation and Sample Analysis. Crystallographic information about the prepared samples was established by powder X-ray diffraction (XRD, Shimadzu, model XRD-6000, Cu Kα radiation, λ = 1.5406 Å). Field emission scanning electron microscopy (FESEM, equipped with STEM function; JSM-6700F, JEOL) was employed to examine the morphologies of the product nanocomposites. Structural and compositional investigations with transmission electron microscopy (TEM), high-resolution TEM (HRTEM), and energy-dispersive X-ray spectroscopy (EDX) were carried out on JEM-2010 and JEM-2100F (JEOL) instruments, operated with an electron kinetic energy of 200 kV. Surface analysis of the samples was performed with X-ray photoelectron spectroscopy (XPS, AXIS-HSi, Kratos Analytical). The X-ray photoelectron spectra of all of the elements of interest were referenced to the C 1s peak arising from adventitious carbon (its binding energy was set at 284.6 eV). The UV−vis absorption spectra of the as-prepared samples in the wavelength range from 200 to 800 nm were recorded on a Shimadzu UV-2450 spectrophotometer. The diluted heterodimers and dumbbell solutions used in the measurement were transparent. Additionally, the transmittance and reflectance spectra were also taken with or without an integrating sphere (Shimadzu ISR-2200). No major difference was found, and therefore light scattering was negligible in our measurements. Furthermore, optical microscopic photographs were taken on an Olympus microscope (BX51) for samples studied in our photo-induced antibacterial tests detailed below.

2.5. Antibacterial Tests with Ag_2S/Ag Heterodimers. *E. coli* K-12 was cultured in a nutrient broth at 37 °C overnight (i.e., 16−18 h) at 200 rpm in a rotary shaker until reaching stationary growth phase. The bacterial cells were collected by centrifugation at 4000 rpm for 10 min, and the bacterial pellets were washed three times with sterilized Milli-Q water to remove residual culture media components. The as-prepared cells were then resuspended and diluted to the required cell density of around 10^7 colony-forming units per milliliter (CFU/mL) with sterilized Milli-Q water. An aliquot of the *E. coli* suspension and a certain amount of the Ag_2S/Ag heterodimers were added to a glass bottle. The final Ag_2S/Ag concentration was adjusted to 0.01 and 0.10 mg/mL, respectively. To generate UV photoirradiation for the bactericidal tests, a high-pressure mercury lamp (Philips HPR 125W) was used as light source in this study. The emission wavelength of the UV lamp peaks at about 365 nm (i.e., UV-A), and its luminous efficacy is around 23.2 lm/W. The light was passed through a UV cutoff filter (λ > 290 nm) and then shone onto a 20 mL reaction beaker that contained the test suspensions described above. The distance between the UV light source and the reaction beaker was ca. 20 cm. Before and during the light irradiation, 0.50 mL aliquots of the reaction mixture were withdrawn at time intervals of 10 min and diluted serially with sterilized Milli-Q water to adjust the bacterial concentration to ensure the growing bacterial colonies were being counted accurately and easily. In this connection, 0.10 mL of the diluted mixture was spread on a nutrient agar medium, and the colonies were counted to determine the viable bacterial numbers after being incubated at 37 °C for 24 h. All of the bactericidal experiments were performed at room temperature and repeated three times in order to give an average value; the measured data for each set of experiments were expressed with the mean and standard deviation. The diluted *E. coli* suspension without addition of the Ag_2S/Ag heterodimers was also irradiated with the same UV light source under identical experimental settings and was used as a control reference. On the other hand, a culture experiment on the reaction mixture (*E. coli* together with Ag_2S/Ag heterodimers) in a rotary shaker at 37 °C without UV light irradiation was also conducted for comparison. For the TEM examination, the specimens were stained with a sodium phosphotungstate aqueous solution for 1 h

(41) Pang, M. L.; Zeng, H. C. *Langmuir* **2010**, *26*, 5963.

and then washed twice with sterilized Milli-Q water. The TEM copper grids were air-dried in a natural laboratory environment and examined using the TEM (JEOL JEM-2010) as described earlier. For optical imaging, *E. coli* and Ag_2S/Ag mixtures were stained by LIVE/DEAD BacLight Bacterial Viability Kits (Invitrogen), and then optical photographs were taken using an Olympus microscope BX51 before and after UV light irradiation. The Bacterial Viability Kits provided two different nucleic acid stains to rapidly distinguish live *E. coli* with intact plasma membranes (green) from dead *E. coli* with compromised membranes (red). Finally, in order to monitor possible dissolution of Ag^+ ions, quantitative analysis of the silver ions eluted from the catalysts was carried out via inductively coupled plasma mass spectrometry (ICP-MS, Agilent 7500). All of the solutions were prepared with sterilized ultrapure water in this investigation, and all the ICP-MS measurements were repeated three times.

3. Results and Discussion

3.1. Synthesis and Morphological Control. According to the schematic illustration in Figure 1, monodisperse solid spheres of Cu_2O and hollow spheres of CuS were first synthesized through a modified Kirkendall process as the starting precursors for our present preparation of Ag_2S/Ag heterodimers. Some typical TEM and HRTEM images for the two types of solid precursors (Cu_2O and CuS) prepared at room temperature can be found in the Supporting Information (SI-1). Interestingly, both types of the spheres are highly uniform, but their outer diameters are in the ranges of 130−135 and 170−180 nm, respectively.[41] We believe that the chemical conversion of Cu_2O to CuS (and similarly CuS to Ag_2S) started from the external surfaces of precursor spheres; that is, the previous solid phase served as a template for a later solid phase to develop, causing a gradual increase in the sphere diameters. The selected area electron diffraction (SAED, SI-1) pattern exhibits diffraction rings, indicating a polycrystalline nature of the as-prepared Cu_2O solid spheres although some discrete diffraction spots can also be observed. Consistent with the discrete diffraction spots, the HRTEM image of Cu_2O solid spheres shows clear lattice fringes and large coherent lattice domains (SI-1). The uniformity of the transformed hollow CuS spheres is also very high (SI-1). The measured lattice fringes marked in the HRTEM images are 0.22 nm for the Cu_2O solid spheres and 0.19 nm for the CuS hollow spheres, which correspond to the d_{200} interplane spacing of cubic Cu_2O and the d_{110} interplane distance of covellite CuS phase, respectively.

Figure 2 shows some representative TEM images of the as-synthesized Ag_2S/Ag heterodimers following the process schemes of Figure 1. In addition to the cationic exchange between Cu^{2+} and Ag^+ that formed hollow spheres of Ag_2S, it is quite intriguing to observe that a small metallic silver particle was also deposited on each hollow sphere of Ag_2S after the $AgNO_3$ was added into the CuS-EtOH-PVP suspension at room temperature (Figure 2a). The resultant hollow asymmetric heterodimers of Ag_2S/Ag were also very uniform and nearly monodisperse at close to 100% morphological yield; a large-scale panoramic view of the overall product is given in the Supporting Information (FESEM image, SI-2). It should be noted that the average outer diameter of the Ag_2S hollow spheres is around 220 nm, which is larger than that of the original CuS hollow spheres, while their simultaneously formed Ag particles have some major crystal sizes ranging from 50 to 75 nm (Figure 2a). Our HRTEM investigation shows some well-resolved lattice fringes corresponding to monoclinic Ag_2S and faced-centered cubic Ag, respectively (SI-3). Two individual parts of the heterodimers, hollow Ag_2S and solid Ag, can be seen clearly from the TEM image of Figure 2b, but the interface between them is not so distinguishable. In order to resolve this uncertainty, detailed information on the structure and local atomic composition of the Ag_2S/Ag heterodimers was further acquired with EDX line scanning and elemental mapping. In Figure 2c, the intensities of the S $K\alpha_1$ signal peak at the shell regions, while there is a dip at the central part, which indeed reveals the formation of hollow structure in the Ag_2S spheres. A similar trend for the Ag $L\alpha_1$ signal profile can also be observed except for a drastic rise at the location of the Ag nanoparticle, which should be ascribed to a sudden increase in silver density from the Ag_2S hollow sphere to the metallic Ag end of the heterodimer. Therefore, both line profiles of Ag and S components along the examined line explicitly reveal the hollow structure of the Ag_2S sphere and its solid Ag counterpart. Furthermore, the atomic ratio of Ag/S measured from the EDX spectrum is 2.76:1 (SI-4), which is much greater than the stoichiometric ratio 2:1 for the phase pure Ag_2S but is consistent with the existence of metallic Ag ends on the Ag_2S spheres. In Figure 2d, elemental mapping study of Ag and S on a single dimer further confirms even distributions of Ag and S in the Ag_2S shell and an abrupt increase of Ag content and a sharp decrease of S on the solid end of the Ag_2S/Ag heterodimer. This finding is in excellent agreement with our TEM/HRTEM observations and EDX line profile results, suggesting that the intimate contact between the hollow Ag_2S and solid Ag may allow effective carrier communication in this biphasic composite.

Together with the diffraction bar patterns from the literature data, Figure 3a reports a series of XRD patterns for the structural evolution from Cu_2O solid spheres to CuS hollow spheres and then to the final product Ag_2S/Ag heterodimers. All the diffraction peaks of the as-prepared Cu_2O and CuS samples agree well with the cubic Cu_2O (JCPDS card no. 34-1354; space group $Pn\bar{3}m$; lattice constant $a_0 = 4.217$ Å) and hexagonal covellite CuS (JCPDS card no. 06-0464; space group $P6_3/mmc$; lattice constants $a_0 = 3.792$ Å and $c_0 = 16.344$ Å), confirming the phase-pure Cu_2O and CuS spheres, respectively.[41] For the Ag_2S/Ag sample, the diffraction peaks can be assigned perfectly to the monoclinic phase of Ag_2S (JCPDS card no. 14-0072; space group $P2_1/n$; lattice constants $a_0 = 4.229$ Å, $b_0 = 6.931$ Å, $c_0 = 7.862$ Å, and $\beta = 99.61°$). Although only the (111) reflection of the Ag phase is observable owing to the small content of the Ag phase (JCPDS card no. 04-0783; space group: $Fm\bar{3}m$, $a_0 = 4.086$ Å) in comparison to the Ag_2S spheres,[42] the presence of single-crystalline metallic Ag ends is unambiguously demonstrated in the HRTEM image displayed in Figure 3b (also see section 3.3 below) and a surface analysis below.

Surface information on the Ag_2S/Ag heterodimers was further acquired with the XPS technique. The peaks at 368.2 and 374.2 eV in the Ag 3d photoelectron spectrum in Figure 3c should be assigned to the binding energies of Ag $3d_{5/2}$ and Ag $3d_{3/2}$ of the metallic Ag^0, respectively.[43,44] On the other hand, the smaller components at 367.8 and 373.8 eV could be attributed to those of Ag $3d_{5/2}$ and Ag $3d_{3/2}$ of Ag^+ ions in the Ag_2S hollow spheres.[43,44] It is understandable that the silver in the outer

(42) Zhang, L. Z.; Yu, J. C.; Yip, H. Y.; Li, Q.; Kwong, K. W.; Xu, A. W.; Wong, P. K. *Langmuir* **2003**, *19*, 10372.
(43) Wagner, C. D.; Riggs, W. M.; Davis, L. E.; Moulder, J. E.; Muilenber, G. E. *Handbook of X-ray Photoelectron Spectroscopy*; Physical Electronics Division, Perkin-Elmer Corp.: Eden Prairie, MN, 1979.
(44) Djoković, V.; Krsmanović, R.; Božanić, D. K.; McPherson, M.; van Tendeloo, G.; Nair, P. S.; Georges, M. K.; Radhakrishnan, T. *Colloids Surf., B* **2009**, *73*, 30.

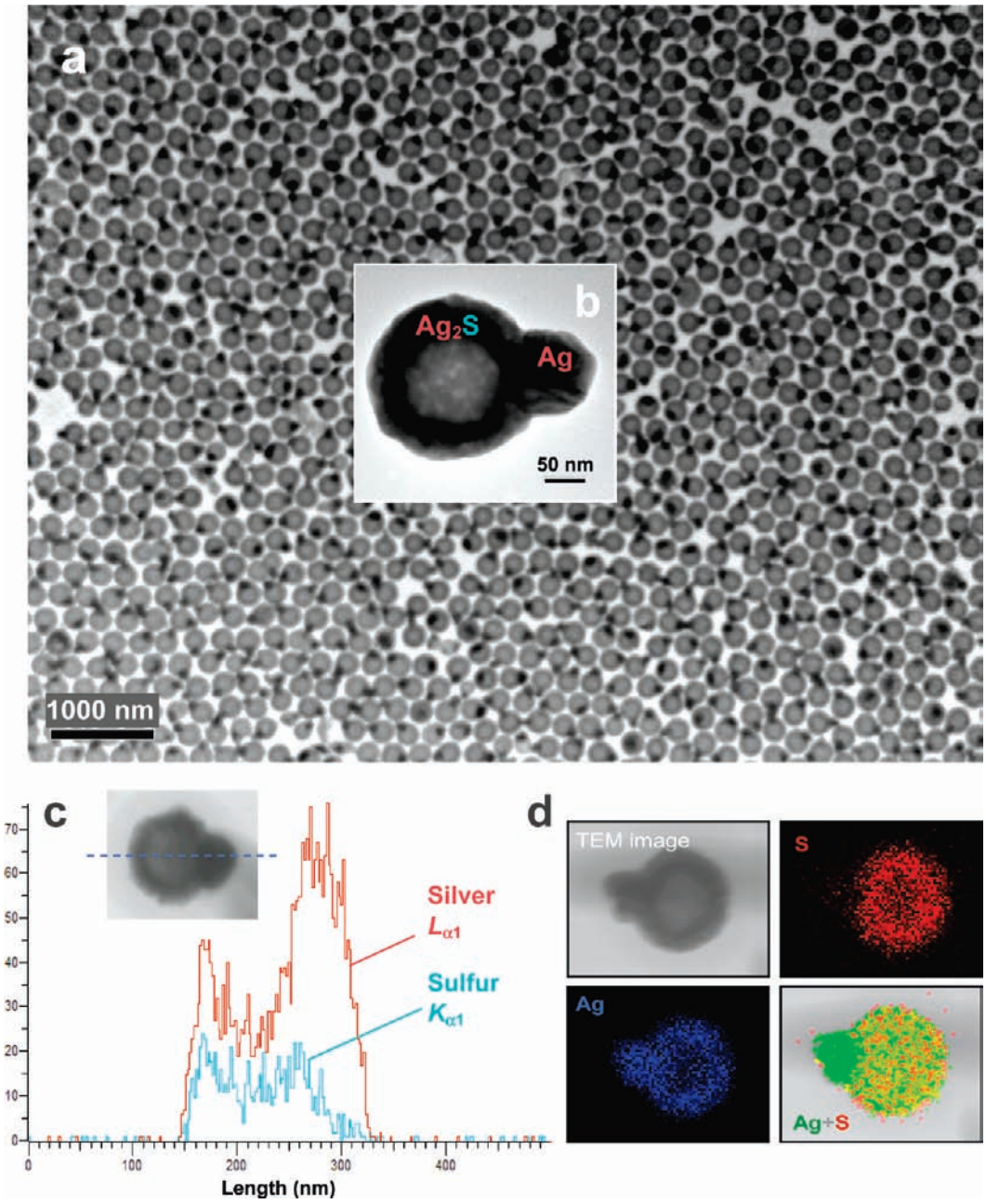

Figure 2. Characterization of Ag_2S/Ag heterodimers: (a) panoramic view of the as-prepared product (TEM image), (b) a detailed view (TEM image), (c) elemental line profiles (see the blue line in the inset TEM image), and (d) elemental mappings of a Ag_2S/Ag heterodimer and its TEM image.

surface region of the Ag_2S/Ag heterodimers was mainly in the metallic state (Ag^0), considering the observed Ag^+ reduction and relative spectral intensities between Ag^0 and Ag^+ components (Figure 3c). The two S $2p_{3/2}$ and S $2p_{1/2}$ peaks located at around 161.5 and 162.7 eV in Figure 3d are assigned to the sulfur anions in the lattice of Ag_2S correspondingly.[43,45] Furthermore, the absence of a Cu 2p signal confirms that the hollow spheres of CuS had been converted essentially into Ag_2S/Ag heterodimers with this wet approach (Supporting Information, SI-4).

3.2. Formation Processes and Mechanistic Study. The conversion of CuS hollow spheres to Ag_2S/Ag heterodimers is believed to be based on a cation-exchange process between Cu^{2+} and Ag^+ and possible reduction processes of Ag^+ ions to Ag^0 with participation of Ag_2S phase. The underlying mechanism related to silver reduction has been investigated in a number of cases in recent years.[37,46−49] Due to an extremely small K_{sp} (1.0×10^{-49}, 18 °C) of Ag_2S, compared to that of CuS (6.3×10^{-36}, 18 °C), the cation-exchange reaction between divalent Cu^{2+} and monovalent Ag^+ could take place instantaneously upon the addition of $AgNO_3$, which has been elucidated by our XRD and XPS results in section 3.1. Several routes may lead to the

(45) Wei, X. M.; Zeng, H. C. *Chem. Mater.* **2003**, *15*, 433.
(46) Robinson, R. D.; Sadtler, B.; Demchenko, D. O.; Erdonmez, C. K.; Wang, L. W.; Alivisatos, A. P. *Science* **2007**, *317*, 355.
(47) Sadtler, B.; Demchenko, D. O.; Zheng, H.; Hughes, S. M.; Merkle, M. G.; Dahmen, U.; Wang, L. W.; Alivisatos, A. P. *J. Am. Chem. Soc.* **2009**, *131*, 5285.
(48) Chen, C.; Wang, L.; Yu, H. J.; Wang, J. J.; Zhou, J. F.; Tan, Q. H.; Deng, L. B. *Nanotechnology* **2007**, *18*, 115612.
(49) Saunders, A. E.; Popov, I.; Banin, U. *Z. Anorg. Allg. Chem.* **2007**, *633*, 2414.

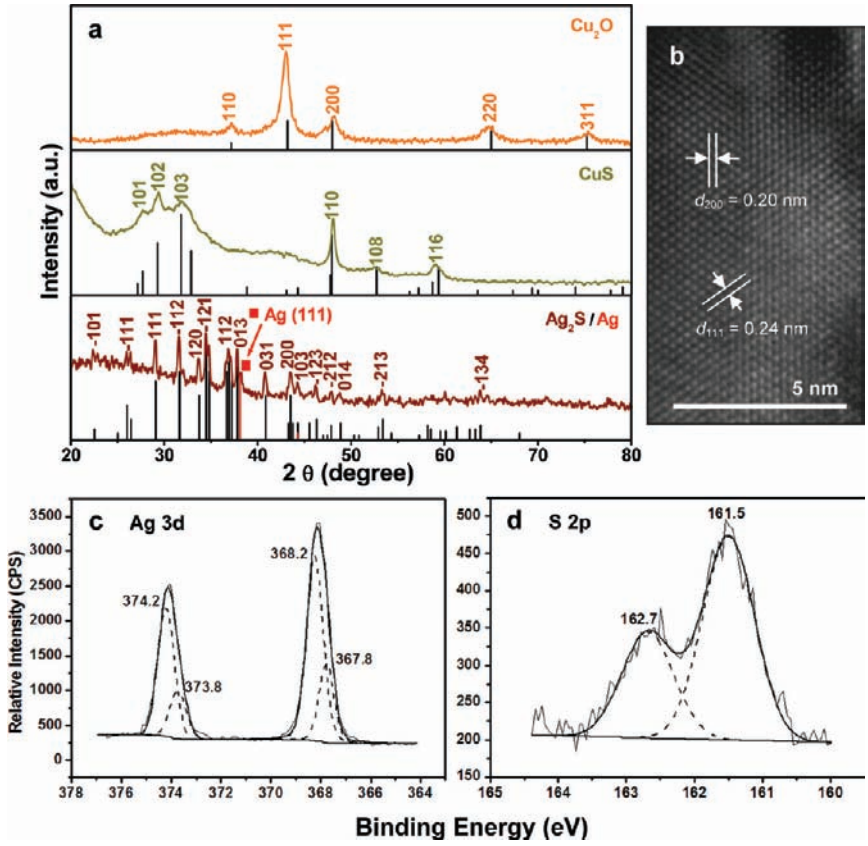

Figure 3. (a) XRD patterns of as-prepared Cu_2O solid spheres, CuS hollow spheres, and Ag_2S/Ag heterodimers, together with their bar patterns from the JCPDS standards (Cu_2O, JCPDS no. 34-1354; CuS, JCPDS no. 06-0464; Ag_2S, JCPDS no. 14-0072; and Ag, JCPDS no. 04-0783), (b) HRTEM image of the Ag phase in the Ag_2S/Ag composite, (c) XPS spectrum of Ag 3d photoelectrons, and (d) XPS spectrum of S 2p photoelectrons of the as-prepared Ag_2S/Ag heterodimers.

reduction of Ag^+ ions under our reaction conditions. For instance, it is well known that $AgNO_3$ in the presence of ethanol and PVP or other nonionic surfactants could be easily reduced to metallic silver nanoparticles.[50−52] Because a similar synthetic environment (i.e., $AgNO_3$ in the presence of ethanol and PVP) was available in this work (see section 2.2), this reduction process should be considered as a viable route to form metallic silver, as depicted in scheme (i) in Figure 1. In the absence of PVP, however, our experiments show that $AgNO_3$ (in deionized water) can react with CuS in either aqueous media or alcohol media (ethanol, methanol, or 2-propanol); however, a lot of irregular Ag nanoparticles together with hollow Ag_2S spheres with very rough surfaces will be produced rather than forming those Ag_2S/Ag heterodimers shown in Figures 2−6. In addition to its reducing capability, the PVP included in the synthesis also possesses regulating/stabilizing ability to restrict random growth and to ensure the formation of Ag_2S/Ag heterodimers with smooth product topology. On the other hand, according to the standard electrode potentials of Ag^+/Ag (+0.7991 V) and S/S^{2-} (−0.44 V), direct redox reaction between Ag^+ and S^{2-} to form metallic silver also seemed to be possible during the ion exchange, especially in the presence of Ag_2S catalyst.[38] Nevertheless, this redox route appeared to be less viable in our synthesis because all the final hollow Ag_2S spheres remained integrated after the ion exchange between Cu^{2+} and Ag^+. If the S^{2-} ions were consumed significantly in forming Ag^0, an integral Ag_2S shell would not have been produced, noting that the CuS precursor was the only source of S^{2-} ions in the present synthesis of Ag_2S. Of course, the formation of a Ag phase would be more rapid if there were a stronger reducing agent in the synthesis (e.g., $NaBH_4$ in scheme (ii) in Figure 1). Furthermore, as to the simultaneous growth of Ag crystals on the Ag_2S surface, a photocatalytic reduction process similar to the previously published results should be highly pausible.[37,48,49] In our current scheme, briefly, by adding $AgNO_3$ into the above reaction system, colloidal hollow spheres of Ag_2S were formed immediately from their precursor CuS at the initial stage. Because Ag_2S is a narrow-band-gap *n*-type semiconductor with strong light-absorbing ability, an exciton will form within the Ag_2S when it absorbs a photon (i.e., because of a small optical band gap in the *n*-Ag_2S phase (∼1.0 eV), visible light photons will be able to provide sufficient energy to generate electron−hole pairs), which may reduce adsorbed ionic Ag^+ to metallic Ag^0.[48] The thus-formed silver cluster then acts as both an electron reservoir and a nuclear seed for the subsequent silver reduction and growth. The silver ions from the bulk solution will be continuously reduced and preferentially grown onto the existing Ag seed, as illustrated in scheme (iii) in Figure 1. Similar to the ripening mechanism investigated for the formation of a single metallic domain rather than heterooligomers on many metal/semiconductor heterostructures,[2,3] we believe that an electron-hopping process might also be operative in producing single-domain Ag^0 in our Ag_2S/Ag if there were smaller metallic

(50) Ayyappan, S.; Gopalan, R. S.; Subbanna, G. N.; Rao, C. N. R. *J. Mater. Res.* **1997**, *12*, 398.
(51) Liz-Marzán, L. M.; Lado-Touriño, I. *Langmuir* **1996**, *12*, 3585.
(52) Wang, Y.; Li, Y.; Yang, S.; Zhang, G.; An, D.; Wang, C.; Yang, Q.; Chen, X.; Jing, X.; Wei, Y. *Nanotechnology* **2006**, *17*, 3304.

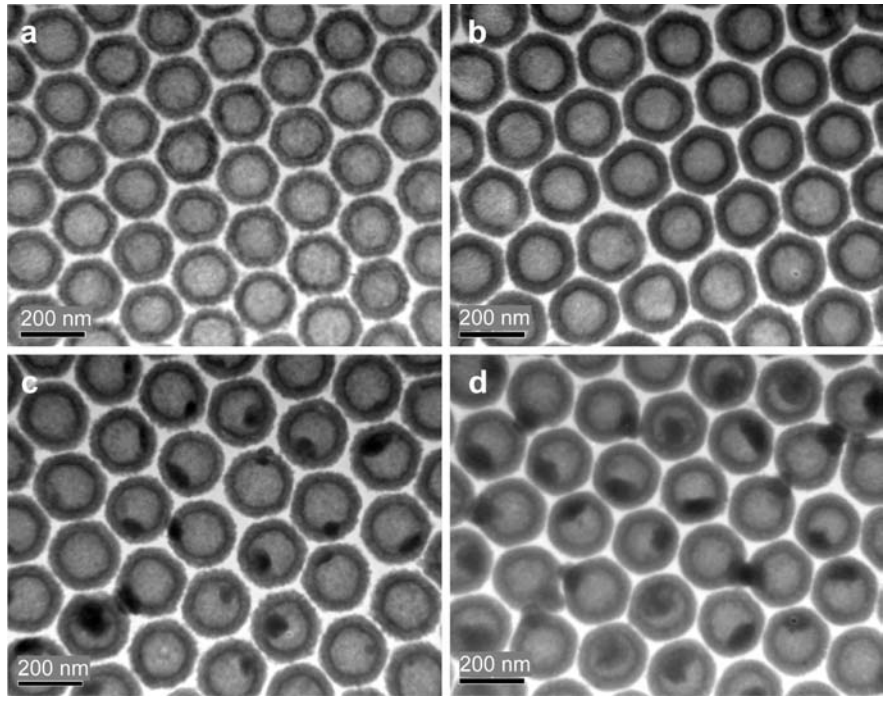

Figure 4. TEM images of hollow spherical products prepared with different molar ratios of $AgNO_3$:CuS (i.e., also the molar ratio of Ag^+:Cu^{2+} or Ag^+:S^{2-}) in the ion replacement synthesis (see Experimental Section): (a) 1:100, (b) 1:10, (c) 1:5, and (d) 2:1. Note that Ag_2S/Ag heterodimers were formed in the latter two cases.

clusters (crystallites) initially formed on the Ag_2S shell surface. To further confirm this reaction route, we carried out comparative experiments with identical synthetic parameters but under darkroom conditions. Nevertheless, only some irregular Ag crystals could be produced together with defective Ag_2S hollow spheres in the absence of visible light. Therefore, the photo-assisted reduction is considered an important part of the synthetic route to generate high-quality Ag_2S/Ag heterodimers.

In order to validate the above proposed mechanisms and confirm that silver particles were produced in wet chemical processes rather than by (TEM) electron beam irradiation in some reported cases,[38,39] several synthetic experiments were carried out as follows. First, we investigated effects of concentration of Ag^+ ions on formation of Ag_2S/Ag heterodimers by varying the molar ratio of $AgNO_3$ to CuS in the starting suspension, as reported in Figure 4. At low molar ratios of $AgNO_3$:CuS from 1:100 to 1:10, only hollow spheres, where Cu^{2+} ions in CuS shells were only partially replaced by the Ag^+, could be observed due to the scarcity of silver ions in the exchange (Figure 4a,b). When the ratio was increased to 1:5, small Ag particles were starting to form on the surfaces of some Ag_2S hollow spheres (Figure 4c). With a further increase in this ratio (i.e., the molar ratio of Ag^+ to S^{2-}) in the precursors to a stoichiometric value of 2:1, the size of the attached Ag nanocrystals increased more noticeably (Figure 4d), and the Ag_2S/Ag heterostructures were formed on individual pristine Ag_2S hollow spheres. Upon further addition of excess $AgNO_3$, however, the size of the Ag ends did not change much, which may be attributable to gradual exhaustion of active consumable reducing species in the precursor solutions. Since the preparation of Ag_2S/Ag heterodimers in this work was conducted in the presence of PVP and ethanol solution, ICP-MS, which requires an aqueous solution environment and without using polymers, appeared not to be very suitable for characterization of our precursor solutions. In order to correlate the compositions of reaction products to their precursors, therefore, a combined EDX and ICP-MS analysis was carried out to determine the molar ratios of Ag:S and Ag:Cu in the final Ag_2S/Ag heterodimers. When the molar ratios of $AgNO_3$:CuS were set at stoichiometric value or higher (2−5), the Ag:S ratios determined by EDX were rather constant, indicating that the Ag_2S/Ag heterodimers were quite similar once they formed under the same set of synthetic parameters, and any excessive Ag^+ ions were left unreacted in the solution. This finding is also supported by our TEM observation in the case of $AgNO_3$:CuS = 5. While the size of the Ag tips in the Ag_2S/Ag heterodimers remained essentially the same, a very small amount of freestanding Ag nanoparticles could be formed at this molar ratio (TEM image; Supporting Information, SI-5), though they would not really affect the final Ag:S ratio. Therefore, the molar ratio of $AgNO_3$:CuS = 5 was considered to be an upper limit for the added $AgNO_3$ in our preparation of Ag_2S/Ag heterodimers. Furthermore, ICP-MS results indicate that the ionic exchange between Ag^+ and Cu^{2+} was rather complete in these processes (Table 1 and SI-4). All these results indicate that the initial growth of the Ag phase was strongly dependent on the amount of the $AgNO_3$ source provided, and this excludes the possibility of electron-beam-induced silver reduction. It should also be mentioned that, due to their relatively large sizes, our as-prepared Ag_2S/Ag heterostructures were in fact quite stable, even when they were

Table 1. Elemental Analysis (EDX and ICP-MS) for Two Reaction Products Prepared with Different Preset Molar Ratios of $AgNO_3$:CuS at 2:1 and 5:1

molar ratio	sample	
$AgNO_3$:CuS in precursor	2:1	5:1
Ag^+:S^{2-} in precursor	2	5
Ag:S (EDX) in product[a]	2.38	2.38
Ag:Cu (ICP-MS) in product[b]	41.11	53.19

[a] The molar ratio determined by EDX method. [b] The molar ratio determined by ICP-MS method (also see Supporting Information, SI-4).

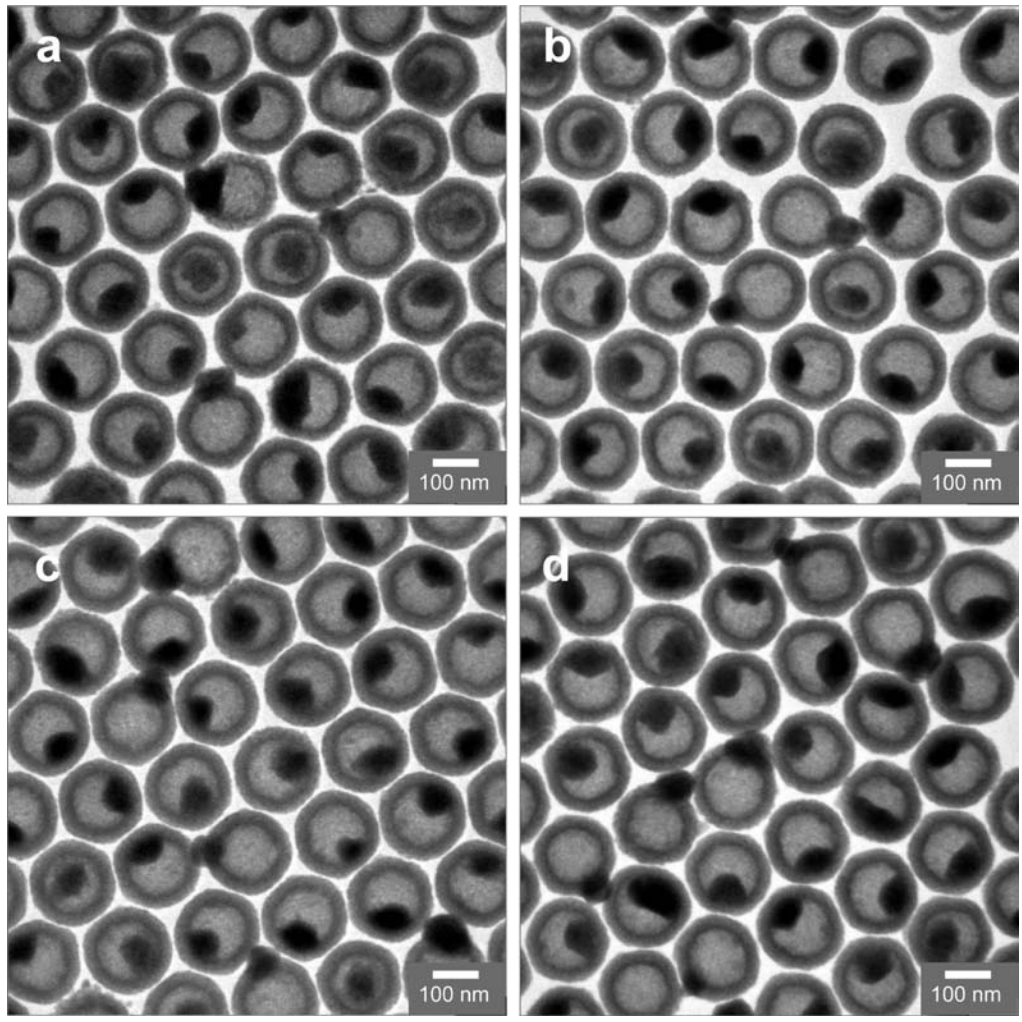

Figure 5. TEM images of hollow Ag_2S/Ag heterodimers prepared at different reaction times: (a) 0, (b) 1, (c) 3, and (d) 10 min.

exposed to the (TEM) electron beam for a long period of time, in contrast to the previous literature results,[38,39] in which an extensive exposure of the Ag_2S nanocrystals to the electron beam led to an increase in the silver metallic cluster size.

Second, we examined the effect of reaction time on formation of Ag_2S/Ag heterodimers. Figure 5 shows TEM images of the samples obtained at different stages of the reaction, in which the ionic ratio of Ag^+:S^{2-} was set at the stoichiometric molar ratio of 2:1. Addition of $AgNO_3$ into the CuS-EtOH-PVP suspension caused an immediate color change from deep blue to black, suggesting uniform Ag_2S/Ag heterodimers were formed instantaneously (Figure 5a). Our TEM images show that there is no significant difference among the samples obtained by adding $AgNO_3$ without further aging ($t = 0$ min, Figure 5a) or with a certain reaction/aging time ($t = 1-10$ min, Figure 5b−d) under stirring conditions, noting that these samples are also quite similar to the one reported in Figure 5d with a longer aging time ($t = 30$ min). In Table 2, the elemental ratios of Ag:S for the samples of Figure 5 measured by EDX method are reported. Consistent with the TEM observation, the Ag:S molar ratios in these samples were almost the same (2.36−2.38), regardless of reaction/aging times (1−30 min). All these observations confirm an instantaneous generation of the Ag_2S/Ag heterodimers upon the addition of $AgNO_3$ solution to the CuS precursor (scheme (i), Figure 1). At the same time, it is further demonstrated that the Ag_2S/Ag heterodimers were very stable once they were

Table 2. EDX Elemental Analysis (Molar Ratio) for Various Reaction Products Prepared with Different Reaction Times

	reaction time (min)[a]				
	0	1	3	10	30
$AgNO_3$:CuS in precursor	2	2	2	2	2
Ag:S (EDX) in product [b]	2.30	2.36	2.37	2.38	2.37

[a] Samples can be referred those in Figure 5. [b] The molar ratio determined by EDX method.

formed (within 1 min). As mentioned earlier, the Ag_2S hollow spheres were enlarged during Ag deposition because the cationic exchange between Cu^{2+} and Ag^+ started from the external surface of the CuS spheres. In agreement with this, the diameters of the Ag_2S hollow spheres in the as-prepared Ag_2S/Ag heterodimers (Figures 4 and 5) seemed to be constant, showing an average value around 200 ± 10 nm. It should be mentioned that due to the formation of hexagonal close-packed superlattices of the hollow spheres in Figures 4 and 5, most Ag^0 tips tend to point toward the air phase in order to reduce their coplanar space during the drying process of our TEM sample preparation. Nevertheless, in Figure 6, these metallic silver tips can be visualized more clearly in the non-close-packed spheres illustrated in our tilt-angle TEM measurements.

Third, we further exploited factors that affect the silver ion reductions. In order to control the size of the Ag phase in the Ag_2S/Ag heterodimers and to demonstrate that the Ag tips were

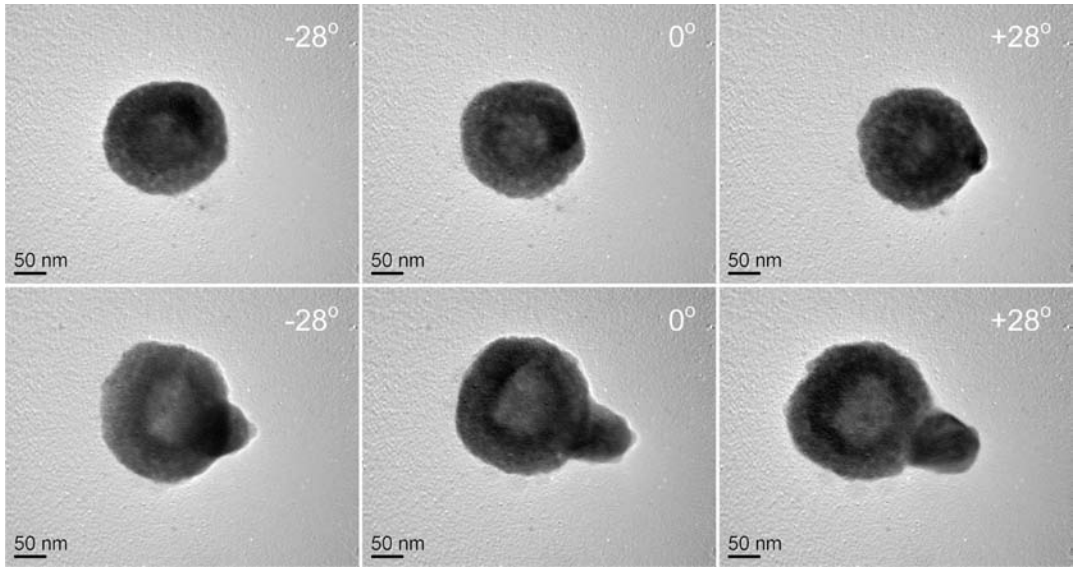

Figure 6. TEM images of two hollow Ag_2S/Ag heterodimers with different tilt angles.

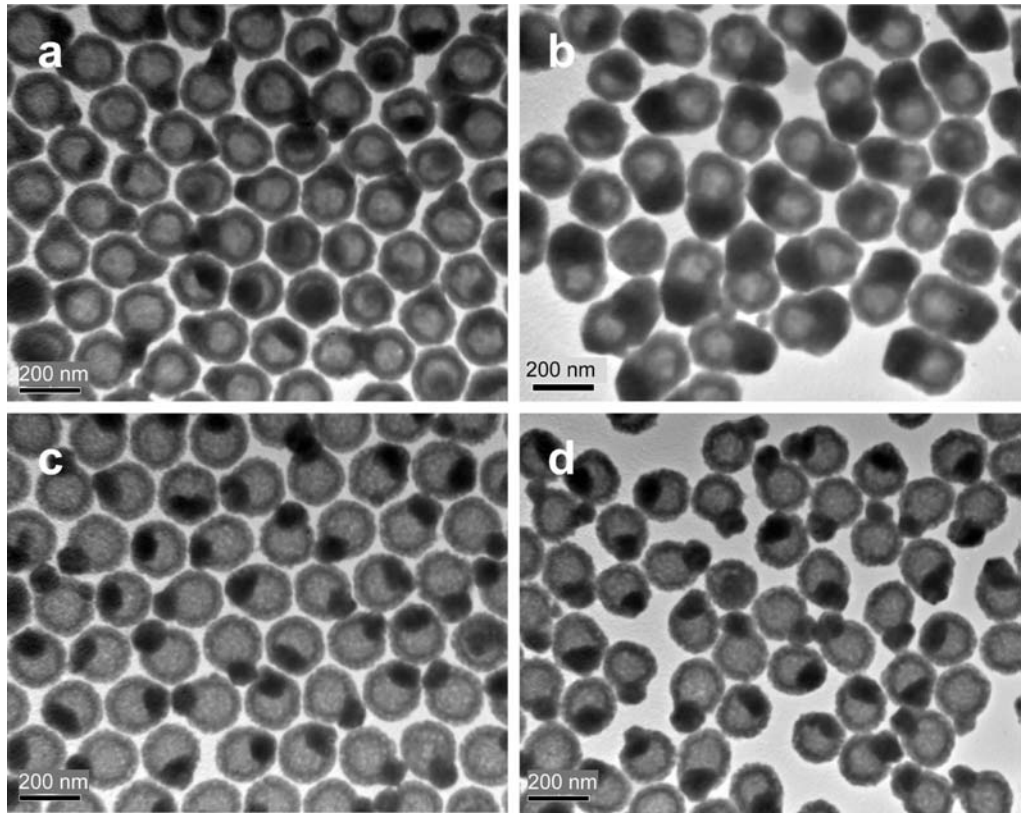

Figure 7. TEM images of hollow Ag_2S/Ag heterodimers prepared with some additional reaction conditions (see Experimental Section): (a) with addition of $NaBH_4$ (0.1 mL, 0.10 M in deionized water) at 60 °C for 1 h, (b) with addition of $NaBH_4$ (0.1 mL, 0.10 M in deionized water) at 60 °C for 4 h, (c) with irradiation of UV light for 1 h, and (d) with irradiation of UV light for 5 h.

formed during the wet chemical synthesis process rather than by electron beam irradiation during TEM measurements, two synthetic schemes were further devised (see section 2.2; schemes (ii) and (iii) in Figure 1): by adding 0.10 mL of $NaBH_4$ (0.10 M in deionized water) into the normal starting suspension (described in the above paragraph and section 2.2) and by irradiating the normal precursor suspension with UV light (Philips high-pressure mercury lamp, 125 W). As is well known, $NaBH_4$ is a strong reductant and widely used in the synthesis of nanoparticles of noble metals.[53] With this reducing agent, the size of the Ag phase can be further controlled. As shown in Figure 7a,b, Ag particles almost equal in size to their Ag_2S counterparts could be prepared with the addition of $NaBH_4$ (at the optimal molar ratio $NaBH_4$:Ag^+ = 1:2) after different reaction times. When the molar ratio of $NaBH_4$:Ag^+ was equal to or greater than 1:1, irregular freestanding Ag nanoparticles were also produced, together with the large-headed Ag_2S/Ag

(53) (a) Ahern, A. M.; Garrell, R. L. *Langmuir* **1991**, *7*, 254. (b) Van Hyning, D. L.; Zukoski, C. F. *Langmuir* **1998**, *14*, 7034. (c) Van Hyning, D. L.; Klemperer, W. G.; Zukoski, C. F. *Langmuir* **2001**, *17*, 3128. (d) Li, J.; Tang, S. B.; Lu, L.; Zeng, H. C. *J. Am. Chem. Soc.* **2007**, *129*, 9401.

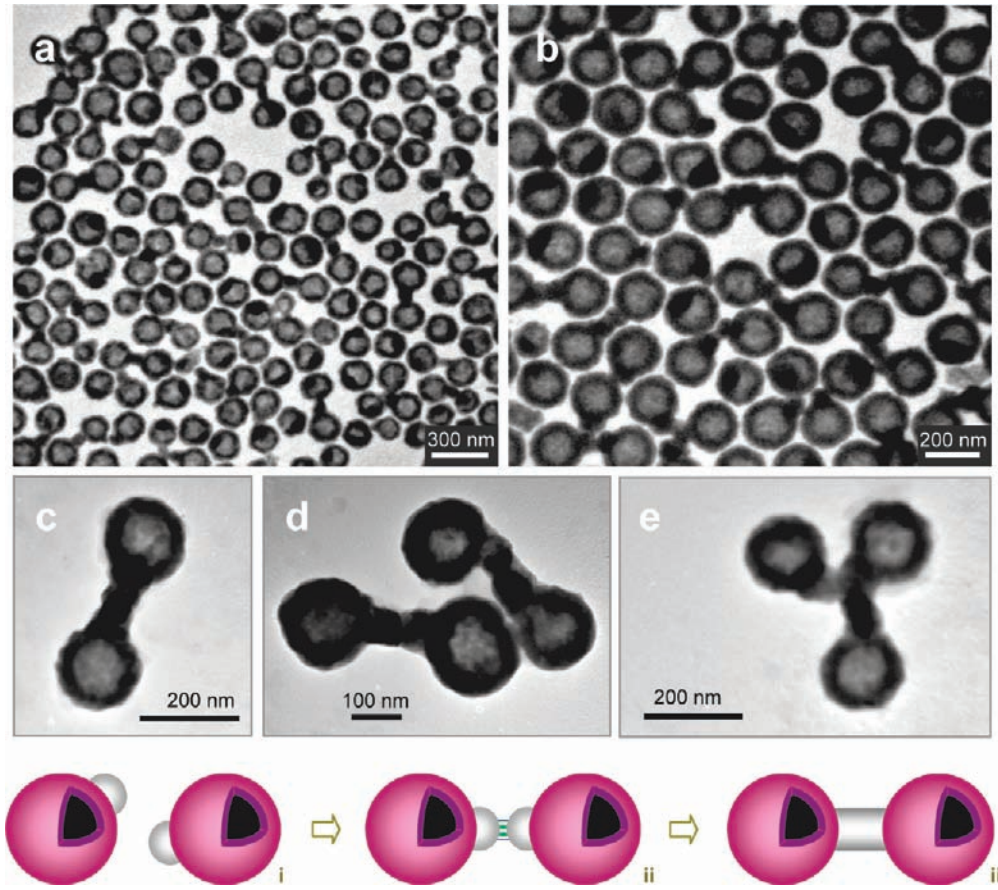

Figure 8. TEM images of hollow $(Ag_2S)_2$/Ag heterotrimers (a−d, together with their starting building units Ag_2S/Ag heterodimers) and $(Ag_2S)_3$/Ag heterotetramers (e). Color illustration indicates the coupling process: (i) randomly oriented heterodimers, (ii) alignment between two heterodimers with assistance of EDA bidentate ligands (blue thin lines between two Ag ends), and (iii) formation of $(Ag_2S)_2$/Ag heterotrimer.

heterodimers (TEM results; Supporting Information, SI-6). On the other hand, photoinduced deposition or photoinduced reduction of Ag^+ is also a versatile synthetic strategy adopted by other researchers.[21,53] Under the irradiation of UV and visible light, similarly, Ag_2S/Ag heterodimers with greater Ag particulate ends could be obtained (Figure 7c,d). The photoinduced reduction in the latter case once again indicates that the Ag nanoparticles were indeed formed during the synthetic processes rather than by the reduction of electron beam irradiation during the TEM measurement. All the investigations and the associated findings confirm the simultaneous generation of Ag_2S hollow spheres and Ag nanoparticles during the formation of Ag_2S/Ag heterostructures.

3.3. Coupling and Tripling of Ag_2S/Ag Heterodimers. In preparation of $Ag_2S/Ag/Ag_2S$ (i.e., $(Ag_2S)_2$/Ag) dumbbells, a small amount of EDA, varying from 0.01 to 0.10 mL, was added into the as-prepared Ag_2S/Ag heterodimers ethanolic suspension (see section 2.2). At room temperature, coupling of Ag_2S/Ag heterodimers was difficult to realize, even with the assistance of EDA, and effective coupling was not observed until the reaction temperature was raised to 60 °C. Figure 8 shows some typical TEM images of the as-obtained $(Ag_2S)_2$/Ag dumbbell-like heterotrimers, in which two individual Ag_2S/Ag heterodimers connected with each other by a newly formed metallic Ag "bar". The coupling yield was as high as ca. 30% in these preliminary trial tests (e.g., Figure 8a−d), noting that occasionally $(Ag_2S)_3$/Ag heterotetramers were also obtained (i.e., tripling of the Ag_2S/Ag heterodimers with a yield of about 5%, Figure 8e). It should be mentioned that EDA is a commonly used chemical in coordination chemistry and controlled growth of nanomaterials. For example, it has been reported that a few diamines, including EDA, can be used as chelating ligands to bind onto silver to form 2D or 3D coordination frameworks.[54] This observation suggests that the observed coupling process was through an "oriented attachment" mechanism.[55−57] Our HRTEM investigation further reveals that the attachment of Ag nanoparticles in this coupling process is along the [111] direction, on the basis of a crystallographic orientation analysis in which lattice fringes of $d_{111} = 0.24$ nm and $d_{200} = 0.20$ nm can be resolved clearly in the boundary regions of the attached Ag nanoparticles (Supporting Information, SI-7). In addition to the direct "oriented attachment", Ostwald ripening was also operative as an underlying mechanism, since the Ag "bar" in the dumbbells became elongated after the coupling process compared to their dimer precursor. In order to understand the role of EDA in the above constructional process, we have tried using alkanethiols or other monoamines (RNH_2) to conduct the

(54) (a) Dai, J.-X.; Zhu, H.-L.; Rothenberger, A.; Zhang, Q. F. *Z. Naturforsch.* **2007**, *62b*, 1112. (b) Pickering, A. L.; Long, D. L.; Cronin, L. *Inorg. Chem.* **2004**, *43*, 4953. (c) Pickering, A. L.; Seeber, G.; Long, D. L.; Cronin, L. *Chem. Commun.* **2004**, 136.
(55) (a) Penn, R. L.; Banfield, J. F. *Science* **1998**, *281*, 969. (b) Penn, R. L. *J. Phys. Chem. B* **2004**, *108*, 12707. (c) Ribeiro, C.; Lee, E. J. H.; Longo, E.; Leite, E. R. *ChemPhysChem* **2005**, *6*, 690. (d) Zeng, H. C. *Int. J. Nanotechnol.* **2007**, *4*, 329. (e) Zhang, Q.; Liu, S. J.; Yu, S. H. *J. Mater. Chem.* **2009**, *19*, 191.
(56) Pacholski, C.; Kornowski, A.; Weller, H. *Angew. Chem., Int. Ed.* **2002**, *41*, 1188.
(57) Liu, B.; Zeng, H. C. *J. Am. Chem. Soc.* **2003**, *125*, 4430.

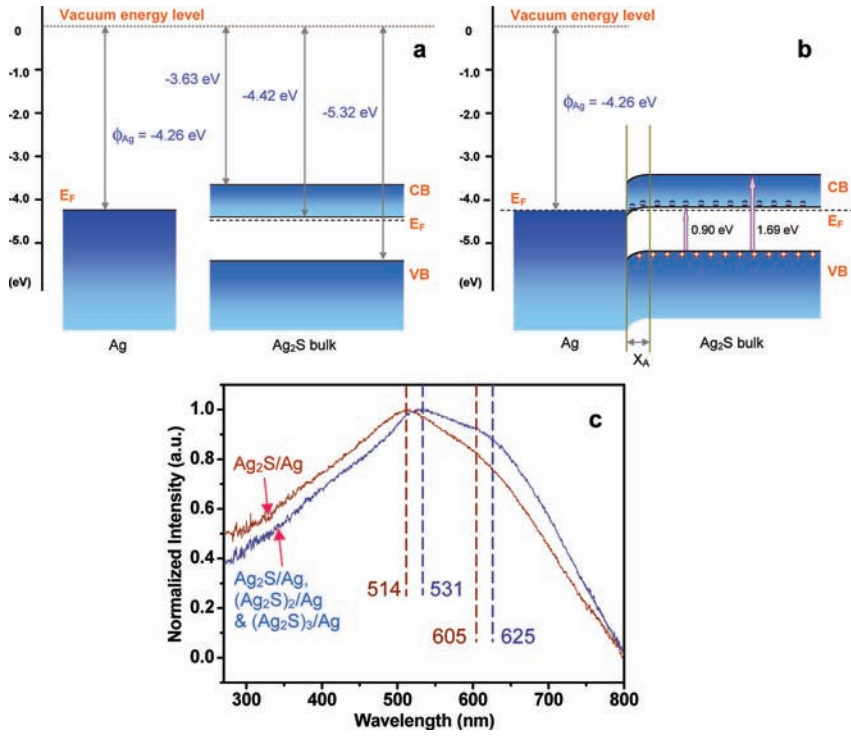

Figure 9. Simplified band structures in the Ag_2S/Ag system (a) before contact and (b) after contact (CB, conduction band; VB, valence band; E_F, Fermi level; ϕ, work function; and X_A, accumulation layer). (c) UV−visible spectra (in transmission mode) for the as-prepared Ag_2S/Ag heterodimers and the mixture of Ag_2S/Ag, $(Ag_2S)_2$/Ag, and $(Ag_2S)_3$/Ag heterostructures.

same experiments under identical conditions; however, no $(Ag_2S)_2$/Ag or $(Ag_2S)_3$/Ag could be obtained. On the other hand, the possible etching of Ag by EDA was not so obvious, although we did observe some ripening modifications of the silver domains (Figure 8). In this regard, the introduction of EDA herein should be ascribed to the favorable adsorption of amine groups than thiol groups on silver surfaces.[58] The bidentate ligand EDA is believed to play an important role in bringing the Ag_2S/Ag building units together. In particular, EDA could work as a linear linker to bridge two Ag_2S/Ag heterodimers via forming $Ag^{\delta+}$:$NH_2CH_2CH_2NH_2$:$Ag^{\delta+}$ surface complex. With these additional Ag···Ag argentophilic interactions, the contact probability of the Ag_2S/Ag heterodimers is enhanced, leading to direct fusion between the two (or even three) silver ends, as shown in the color illustration in Figure 8.

3.4. UV−Vis Measurement. In order to understand the charge transfer within the Ag_2S/Ag system, simplified band structures of the two materials before and after contact are depicted in Figure 9a,b. As can be seen, the work function of silver metal and the bottom of the conduction band of Ag_2S are −4.26 and −4.42 eV from the vacuum energy level.[59] Upon the contact, the electrons (majority carriers) will flow from the Fermi level of the metal (Ag) to the Fermi level (E_F, which is approximately treated as the donor level) of the *n*-type semiconductor (Ag_2S), leaving some positive charge buildup on the metal contact interface. The electrons in the conduction band of Ag_2S can now move to the Ag side more easily, due to the attraction of the opposite charge buildup (see the downward band bending and carrier accumulation layer X_A in Figure 9b), whereas the holes in the valence band experience an energy barrier to travel to the metal side. According to the literature data,[59] there are two major photon-promoted electron transitions in Ag_2S: from the valence band to the bottom energy level and to the dominant energy level, located at −3.63 eV from the vacuum energy level (Figure 9a) within the conduction band (i.e., 0.90 and 1.69 eV, respectively, Figure 9b). Two UV−vis absorption spectra for the Ag_2S/Ag heterodimers (100%) and the sample of Figure 8 (i.e., a mixture containing 65% of Ag_2S/Ag, 30% of $(Ag_2S)_2$/Ag, and 5% of $(Ag_2S)_3$/Ag heterostructures) are displayed in Figure 9c. As noble metals, Au and Ag nanoparticles often exhibit strong surface plasmon resonance (SPR) due to the collective oscillation of conduction electrons exposed to an external electromagnetic field. Similar to the previously published results for Ag_2S,[37] the UV−vis spectrum exhibits only a broad absorption band centered around 514 nm, but the SPR peak around 600 nm, which is normally ascribed to silver nanoparticles having a spatial regime similar to that of our silver products (50−75 nm), is only detected as a small shoulder.[60,61] The weak SPR observed herein indeed suggests that the good contact between the Ag_2S and Ag segments might ensure an effective charge transfer across the phase boundary. When the populations of coupled and tripled structures in the sample was increased, the absorption band and the SPR peak move to the longer wavelength region at 531 and 625 nm, respectively. The observed red-shifts may reflect both grain/crystallite growth of the Ag_2S shells during the heating processes (60 °C) and enlargement of the Ag domains in the final heterostructures. The reported optical band gaps of bulk crystal Ag_2S are about 0.9−1.0 eV at room temperature,[37,59] and those of nanostructured or thin-film Ag_2S are in the range of 1.4−2.3 eV.[62−64] Therefore, the broad absorptions (peaked at 514−531 nm; ∼2.3 eV) can be loosely associated with the primary absorptions of

(58) Hiramatsu, H.; Osterloh, F. E. *Chem. Mater.* **2004**, *16*, 2509.
(59) Levy, B. In *Photochemical Conversion and Storage of Solar Energy*; Pelizzetti, E., Schiavello, M., Eds.; Springer: New York, 1990; p 380.
(60) Lee, K.-C.; Lin, S.-J.; Tsai, C.-H.; Lu, Y.-J. *Surf. Coating Technol.* **2008**, *202*, 5339.
(61) Evanoff, D. D., Jr.; Chumanov, G. *Chem. Phys. Chem.* **2005**, *6*, 1221.

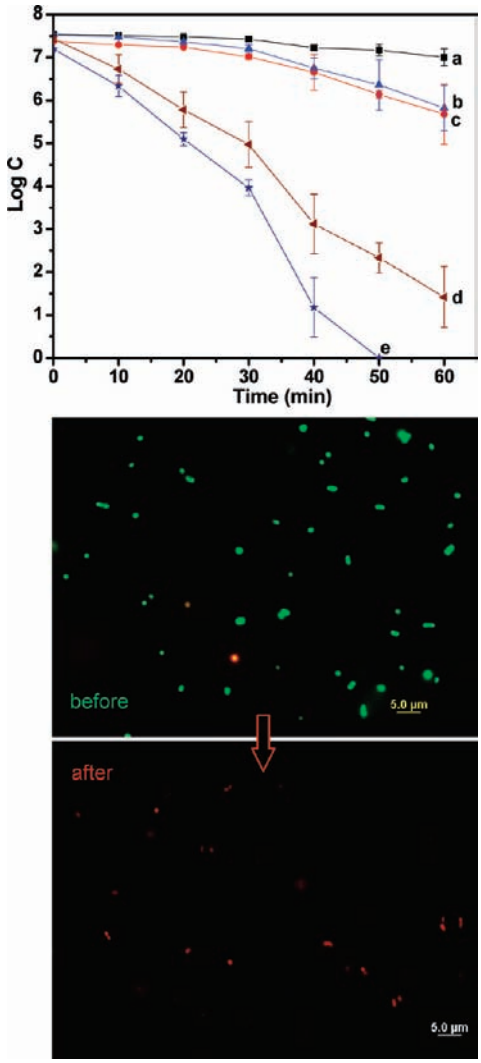

Figure 10. Investigation of the inactivation efficiency against *E. coli* K-12: (a) *E. coli* suspension without Ag_2S/Ag used as a control, (b) *E. coli* suspension without Ag_2S/Ag irradiated by UV light, (c) *E. coli* suspension with 0.10 mg/mL Ag_2S/Ag incubated in a rotary shaker at 37 °C, (d) *E. coli* suspension with 0.01 mg/mL of Ag_2S/Ag dimers under UV irradiation, and (e) *E. coli* suspension with 0.10 mg/mL of Ag_2S/Ag dimers under UV irradiation. Two photographs were taken for *E. coli* K-12 together with Ag_2S/Ag dimers before and after UV irradiation for 1 h.

the valence electrons to various energy states in the conduction band (Figure 9b). Nonetheless, because we were not able to decouple the Ag^+ ion exchange and Ag^0 growth, as discussed in section 3.2, it was not our intention to determine the optical band gap of Ag_2S hollow spheres in this research.

3.5. Photocatalytic Antibacterial Properties. Concerning the prospective applications of this new type of hollow heterodimers, the photocatalytic antibacterial properties of our Ag_2S/Ag heterodimers were also investigated in the present work. Figure 10 shows several plots of $\log_{10} C$ (viable colonies of *E. coli*) versus process time in our antibacterial study. Comparing Figure 10a−c, UV irradiation alone did not show significant bactericidal effects on *E. coli* (case b). Similarly, addition of Ag_2S/Ag heterodimers (0.10 mg/mL) in the absence of UV irradiation made little difference, only 1.7 $\log_{10}$ units of inactivation of *E. coli* being observed in 60 min (case c). The observed low antibacterial activity should be ascribed to the relatively large Ag particles (i.e., 50−75 nm) in our Ag_2S/Ag heterodimers. In this relation, it has been reported that the antibacterial activity of Ag nanoparticles is dependent on the size of the silver particles, with smaller particles having higher activities when an equivalent amount of silver mass is compared.[65,66] Without UV irradiation, therefore, the Ag_2S/Ag heterodimers alone are not particularly toxic to the *E. coli* cells. A remarkable enhancement of inactivation efficiency was obtained by combining Ag_2S/Ag heterodimers with UV light irradiation. Under UV irradiation, about 6.0 $\log_{10}$ units of inactivation of *E. coli* was achieved within 60 min using 0.01 mg/mL of Ag_2S/Ag heterodimers (case d). Increasing the Ag_2S/Ag concentration to 0.10 mg/mL, the *E. coli* cells could be completely inactivated within 50 min (case e). As mentioned in section 3.2, it seems impossible for us to prepare bare Ag_2S hollow spheres without a Ag domain by our present method. On the other hand, there have not been any reports on the antibacterial properties of Ag_2S nanomaterials. Therefore, we believe that the observed bactericidal activity of Ag_2S/Ag heterodimers against *E. coli* K 12 in the presence of UV irradiation should be attributed to the synergetic effects of both Ag_2S and Ag phases. The above findings were also confirmed by the fluorescence label method using a live-and-dead kit on the *E. coli* cells before and after UV irradiation (see section 2.5). The optical microscopic images in Figure 10 present some results of our antibacterial tests for *E. coli* in the presence of Ag_2S/Ag under UV light irradiation using process conditions similar to case e. The live *E. coli* cells before the irradiation and dead cells after the irradiation can be identified respectively in green and red in these images.

To understand the roles of Ag_2S/Ag heterodimers in the above-described photocatalytic processes, the morphological evolution of *E. coli* at different UV exposure times was investigated. Figure 11a shows a TEM image of untreated *E. coli* (incubated overnight) before light irradiation. The pristine *E. coli* possessed a well-defined cell wall and an evenly distributed interior content, indicating that the structural integrity of the bacteria was maintained and intracellular components such as proteins and DNA remained essentially intact. However, as shown in Figure 11b, a significant morphological change occurred after the *E. coli* cells were mixed with the Ag_2S/Ag heterodimers and underwent UV treatment for 1 h. In particular, the Ag_2S/Ag dipolar particles adhered onto the cell walls of *E. coli* tightly, causing the cytoplasmic membranes to shrink and detach from the cell walls. Apparently, part of the *E. coli* cells were damaged and the general (TEM) image contrasts of the cells were lightened, suggesting that the outer membrane of *E. coli* was no longer intact and the interior substances of the cells leaked out. This lysis phenomenon can be seen more clearly from the TEM images of the mixture of *E. coli* and Ag_2S/Ag with a longer UV treatment. Upon increasing the irradiation time to 1.5 h (Figure 11c), the hollow regions extended farther

(62) (a) Wada, Y.; Kaneko, M.; Niinobe, D.; Tsukahara, Y. *Chem. Lett.* **2005**, *34*, 1618. (b) Anthony, S. P. *Mater. Lett.* **2009**, *63*, 773. (c) Grozdanov, I. *Appl. Surf. Sci.* **1995**, *84*, 325. (d) Chen, R.; Nuhfer, N. T.; Moussa, L.; Morris, H. R.; Whitmore, P. M. *Nanotechnology* **2008**, *19*, 455604.
(63) Kryukov, A. I.; Zin'chuk, N. N.; Korzhak, A. V.; Kuchmii, S. Ya. *Theor. Exp. Chem.* **2001**, *37*, 296.
(64) Motte, L.; Billoudet, F.; Pileni, M. P. *J. Phys. Chem.* **1995**, *99*, 16425.
(65) Panáček, A.; Kvítek, L.; Prucek, R.; Kolář, M.; Večeěová, R.; Pizúrová, N.; Sharma, V. K.; Nevěčná, T.; Zbořil, R. *J. Phys. Chem. B* **2006**, *110*, 16248.
(66) Lok, C.-N.; Ho, C.-M.; Chen, R.; He, Q.-Y.; Yu, W.-Y.; Sun, H. Z.; Tam, P. K.-H.; Chiu, J.-F.; Che, C.-M. *J. Biol. Inorg. Chem.* **2007**, *12*, 527.

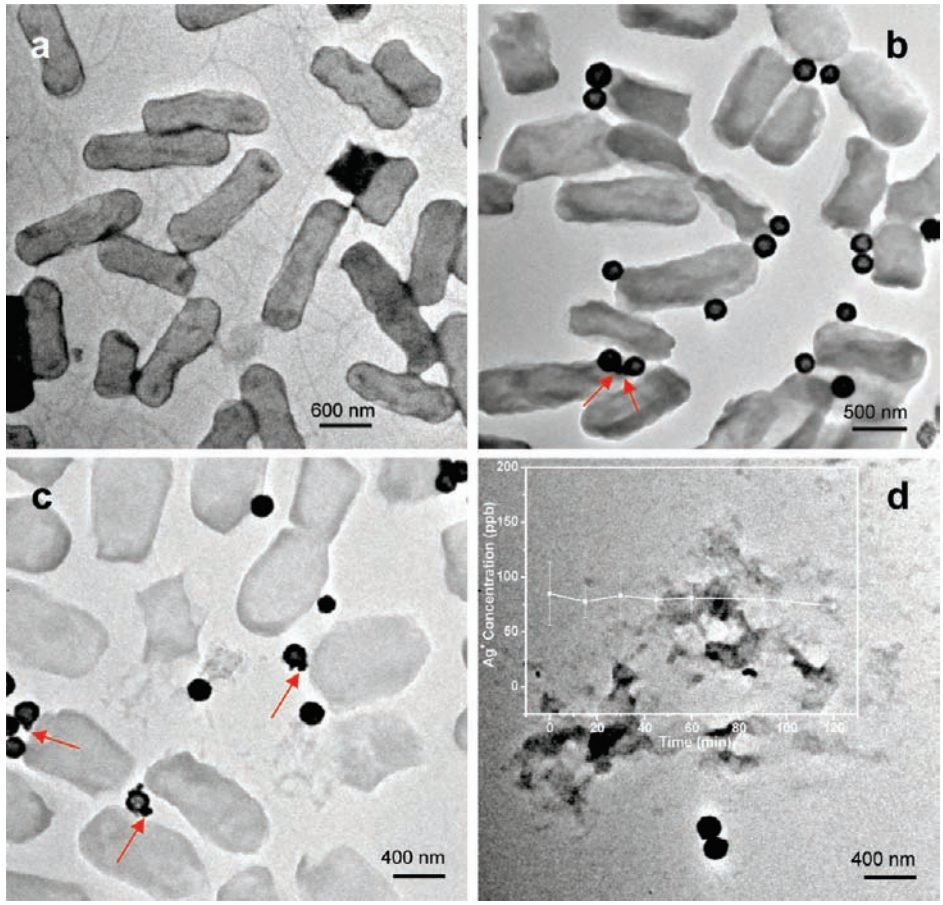

Figure 11. TEM images of (a) as-obtained *E. coli* (incubated overnight) and *E. coli* together with the anchored Ag_2S/Ag heterodimers after different UV irradiation times: (b) 1, (c) 1.5, and (d) 2 h. Some obvious Ag ends on the Ag_2S/Ag heterodimers are indicated with red arrows. Inset in (d) indicates the constant concentration of Ag^+ ions at 75 ppb during the bactericidal process (2 h).

and the morphological changes appeared in almost all of the cells. After UV irradiation for 2 h (Figure 11d), all the pristine cells disappeared completely, leaving only a large number of fibriform cell fragments. As can be seen from these TEM images, the Ag_2S/Ag photocatalysts exhibit good stability under prolonged UV irradiation, and no obvious solid dissolution was found throughout the bactericidal processes. In order to confirm the above observation and exclude possible dissolution of Ag^+ ions from the above Ag_2S/Ag photocatalysts, we further used ICP-MS to monitor the Ag^+ ion concentration during the bactericidal processes. The inset of Figure 11d reports Ag^+ ion concentration in the *E. coli* suspensions with 0.10 mg/mL of Ag_2S/Ag heterodimers under different UV irradiation times. It can be seen from these ICP-MS data that the Ag^+ concentration remained at an extremely low level of only around 75 parts per billion (ppb) and did not change noticeably over the entire photocatalytic process. Apart from the ICP-MS analysis, we also employed EDX technique to determine the molar ratios of Ag:S for the used catalysts. For example, the measured molar ratio of Ag:S of the Ag_2S/Ag heterodimers after irradiation by UV light for 2 h (in the presence of *E. coli* fibriform cell fragments) was 2.37, which was almost identical to the value (2.38) before its use in photocatalytic reactions. On the basis of both ICP-MS and EDX results, we can thus conclude that essentially no Ag^+ ions were released from the Ag_2S/Ag catalyst samples into the solution phase in the bactericidal processes. As reported in Figure 12, a similar trend was also observed upon treatment of the *E. coli* cells with a shorter incubation time (i.e., 4 h, at which time the bacteria were in an exponential growth phase and their cells had a higher aspect ratio). All these observations collectively demonstrate that the inactivation and associated death of *E. coli* cells should be largely attributed to the destruction of their outer membrane. At this stage of research, the observed bactericidal process can be summarized in three steps. Briefly, the *E. coli* cell walls were first damaged in the presence of the Ag_2S/Ag, followed by discharge of intracellular substances, and finally the whole cells collapsed and fragmented.

It is noted that the mechanisms underlying the bactericidal activity of silver ions and silver-containing materials have remained unclear and controversial so far.[67−69] One possibility is that the growth inhibitory or bactericidal effects may be related to the formation of free radicals from the surfaces of the Ag phase. These reactive free radicals can attack membrane lipids and cause a breakdown of the function of cell membranes.[68] In this connection, Figures 11 and 12 indicate that the Ag_2S/Ag heterodimers are efficient catalysts for inactivation of *E. coli*, and their bactericidal effects on *E. coli* can be ascribed to photocatalytic processes. In particular, the bactericidal effect of the Ag_2S/Ag photocatalyst may be attributed to destruction of the cell walls by various reactive oxygen species such as superoxide radicals and hydroxyl radicals rather than by intrinsic cytotoxicity of Ag ions eluted from the compounds into the system containing the microorganisms,[67−72] because our Ag_2S/Ag samples exhibited good stability under prolonged UV

(67) Chang, Q. Y.; He, H.; Ma, Z. C. *J. Inorg. Biochem.* **2008**, *102*, 1736.
(68) Mendis, E.; Rajapakse, N.; Byun, H. G.; Kim, S. K. *Life Sci.* **2005**, *77*, 2166.
(69) Kim, J. Y.; Lee, C.; Cho, M.; Yoon, J. *Water Res.* **2008**, *42*, 356.

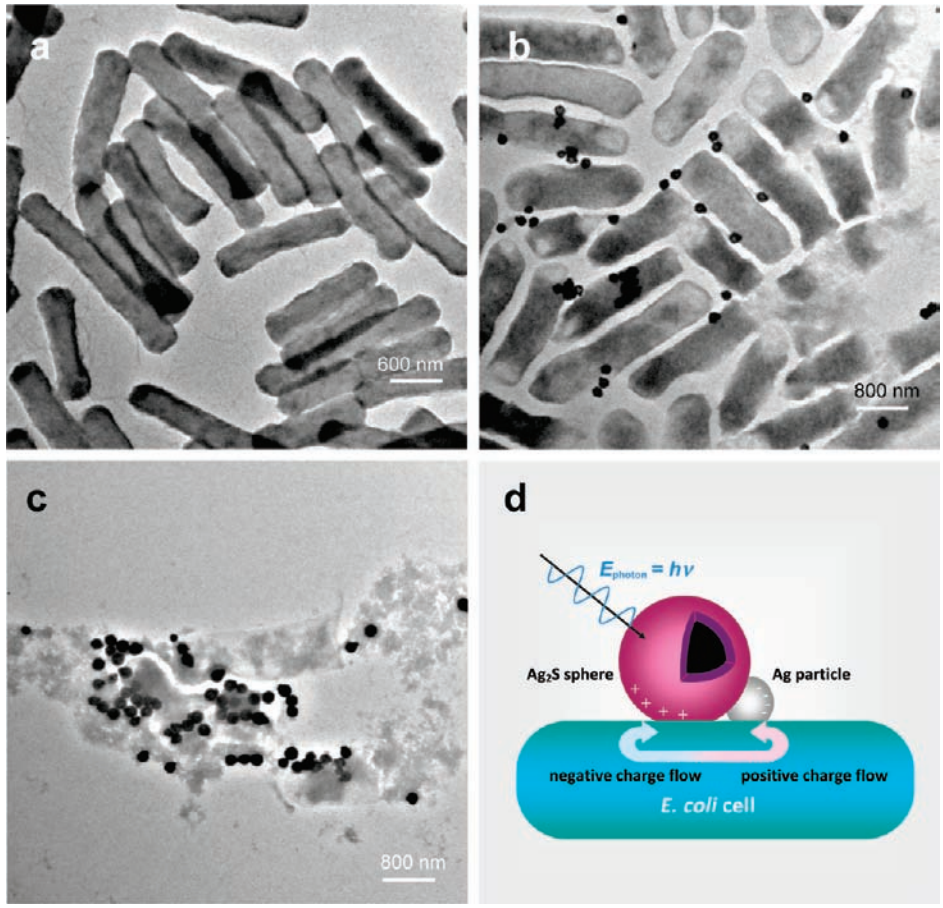

Figure 12. TEM images of (a) as-obtained *E. coli* (incubated for only 4 h) and *E. coli* together with the anchored Ag_2S/Ag heterodimers after different UV irradiation times: (b) 1 and (c) 2 h. Color illustration in (d) depicts a possible mechanism for bacterium inactivation with the surface-anchored Ag_2S/Ag heterodimers. With the injection of UV light energy and charge separation, a closed intracellular circuit loop may be formed with the anchored surface dimer, which enhances lysis of the bacterial cell.

irradiation and no appreciable solid dissolution was found throughout the bactericidal processes (i.e., ICP-MS and EDX results discussed above). Interestingly, the Ag_2S/Ag heterodimers anchored closely onto the outer walls of *E. coli* cells; this close-contact configuration may further enhance the photocatalytic activity of this bipolar composite (more TEM images of this type can be found in the Supporting Information, SI-8). As illustrated in Figure 12d, a closed intracellular circuit loop with anchored Ag_2S/Ag heterodimers might be generated, resulting in easy evacuation of the lysates such as damaged DNA molecules, ribosomes, cytoplasm, and potassium ions as well as lipopolysaccharide molecules and membrane proteins in addition to the formation of oxidative free radicals on the surfaces.[73,74] Nevertheless, since the present work is focused only on the synthesis and initial exploratory applications of the Ag_2S/Ag heterodimers, further mechanistic verification of their bacterial growth inhibitory and bactericidal effects will be required in future investigations of this system. For example, it is our belief that thiol groups of the membrane proteins may bond well to the surface Ag_2S/Ag heterodimers due to their elemental similarity. The actual bonding nature could be a challenging research topic toward a general understanding of the bactericidal activity of the studied materials system.

4. Conclusions

In summary, hollow/solid Ag_2S/Ag heterodimers can be synthesized at room temperature using our wet-chemical method through synthesis of monodisperse Cu_2O solid spheres, conversion of the Cu_2O to CuS hollow spheres, and ion-exchange of the resultant CuS to Ag_2S hollow spheres. On the other hand, the formation of a metallic silver phase on the resultant Ag_2S can be attributed to photocatalytic reduction in which the Ag_2S phase serves as a catalyst. It is found that the formation of Ag_2S/Ag heterodimers is instantaneous. In particular, the size of Ag nanocrystals on the hollow Ag_2S spheres can be tuned facilely by changing the concentration and power of reducing agents used in the synthesis, and the growth of Ag phase in the dimers is along the [111] crystallographic direction of silver metal. With the assistance of the bidentate ligand ethylenediamine, linear dumbbell-like $(Ag_2S)_2$/Ag heterotrimers can be prepared via an oriented attachment process at 60 °C, with a high yield of ca. 70%. Similarly, triangular coplanar heterotetramers of $(Ag_2S)_3$/Ag can also be obtained despite a much lower population. The optical absorption of the Ag_2S/Ag heterodimers peaks at 514−531 nm, while a weak shoulder of surface plasma reso-

(70) Chen, M. X.; Yan, L. Z.; He, H.; Chang, Q. Y.; Yu, Y. B.; Qu, J. H. *J. Inorg. Biochem.* **2007**, *101*, 817.
(71) Elahifard, M. R.; Rahimnejad, S.; Haghighi, S.; Gholami, M. R. *J. Am. Chem. Soc.* **2007**, *129*, 9552.
(72) Pratap Reddy, M.; Venugopal, A.; Subrahmanyam, M. *Water Res.* **2007**, *41*, 379.
(73) Stoimenov, P. K.; Klinger, R. L.; Marchin, G. L.; Klabunde, K. J. *Langmuir* **2002**, *18*, 6679.
(74) Heefner, D. L. *Mol. Cell. Biochem.* **1982**, *44*, 81.

nance is observed around 605−625 nm, which indicates a viable carrier communication between the Ag_2S and Ag phases in the dimers. The highly asymmetric heterodimers have exhibited strong bactericidal effects on *E. coli* K-12 upon UV light irradiation. They have also shown good chemical stability under prolonged UV irradiation. Instead of an intrinsic cytotoxicity of Ag ions, therefore, surface reactive oxygen species are believed to be responsible for the damage to the cell walls and the associated cell death. On the basis of our antibacterial experiments and TEM examination, effective anchorage of Ag_2S/Ag to the cell surfaces also contributes to the high bactericidal activity, apart from the surface oxidation. The observed enhancement of photocatalytic activity of this bipolar composite can be ascribed to easy evacuation of the lysates from the cells, as a closed intracellular circuit loop could be formed when the UV energy is harvested with the surface-anchored Ag_2S/Ag heterodimers.

Acknowledgment. The authors gratefully acknowledge financial support provided by National University of Singapore, Economic Development Board, Singapore, and King Abdullah University of Science and Technology, Saudi Arabia. The authors also thank Ms. Xiaolan Tan of Division of Environmental Science and Engineering, Faculty of Engineering, National University of Singapore, for assistance with microbial experiments and discussion.

Supporting Information Available: FESEM image, EDX analysis, HRTEM/FFT images and analysis, and complete ref 15. This material is available free of charge via the Internet at http://pubs.acs.org.

JA102105Q